Geochimica et Cosmochimica Acta 348 (2023) 296–308

Contents lists available at ScienceDirect

Geochimica et Cosmochimica Acta

journal homepage: www.elsevier.com/locate/gca

Reinterpreting radiocarbon records in bamboo corals – New insights from the tropical North Atlantic

Qian Liu [a,*], Laura F. Robinson [a], Erica Hendy [a], Maria G. Prokopenko [b], Joseph A. Stewart [a], Timothy D.J. Knowles [c], Tao Li [d], Ana Samperiz [e]

[a] School of Earth Sciences, University of Bristol, Bristol BS8 1RJ, UK
[b] Department of Geology, Pomona College, Claremont, CA 91711, USA
[c] Bristol Radiocarbon Accelerator Mass Spectrometry, University of Bristol, Bristol BS8 1UU, UK
[d] State Key Laboratory of Palaeobiology and Stratigraphy, Nanjing Institute of Geology and Palaeontology, Chinese Academy of Sciences, Nanjing 210008, China
[e] School of Earth and Environmental Sciences, Cardiff University, Cardiff CF10 3AT, UK

ARTICLE INFO

Article history:
Received 28 March 2022
Accepted 15 March 2023
Available online 21 March 2023
Associate editor: Hao-Jia (Abby) Ren

Keywords:
Deep-sea bamboo corals
Organic node
Bomb radiocarbon (^{14}C)
Deep chlorophyll maximum
Tropical Atlantic

ABSTRACT

Deep-sea bamboo corals (family Isididae) have been used as archives for reconstructing changes in the past ocean. However, uncertainties remain regarding the interpretation of geochemical signals from their organic nodes, specifically the water depth of the signals recorded by the coral. Here we explore this question by measuring radiocarbon (^{14}C) and nitrogen (^{15}N) isotopic compositions of the organic nodes in six bamboo corals collected from the central and eastern tropical Atlantic between 700 m and 2000 m water depth. By comparing coral ^{14}C to measured seawater data, regional shallow-water coral records and climate-model outputs, we find contrasting results between the two regions. Our bamboo coral ^{14}C results from the eastern tropical Atlantic support previous studies that suggest organic node carbon is sourced primarily from the mixed layer of the ocean. By contrast, the ^{14}C of bamboo coral organic nodes from the oligotrophic central Atlantic better correlates with the ^{14}C content of the subsurface deep chlorophyll maximum layer rather than the surface mixed layer. Combined with nitrogen isotope data, this observation suggests that sinking and/or ambient zooplankton feeding on phytoplankton from the deep chlorophyll maximum layer can contribute a significant proportion of the diet of bamboo corals. These results suggest that the carbon source for bamboo corals organic nodes may not always reside in the mixed layer, especially in oligotrophic regions, which has implications for ^{14}C-based age model development in bamboo corals.

1. Introduction

With growing interest in ocean-climate interactions in response to recent anthropogenic warming (e.g., Brown et al., 2019; Bryden et al., 2005; Hobbs et al., 2021; Ummenhofer et al., 2021), high-resolution records (e.g. annual to decadal) of past ocean variability over the last century are becoming ever more valuable. Among these records, radiocarbon (^{14}C) plays an important role in exploring the anthropogenic influence on ocean circulation. Deep-sea corals have the potential to provide archives of geochemical information for past ocean environment and circulation reconstructions (Geyman et al., 2019; Sherwood et al., 2011; Thresher and Fallon, 2021). In particular, bamboo corals (family Isididae) create well-preserved archives to construct continuous high-resolution records of past ocean environments. They have a distinct bamboo-like morphology: a jointed skeleton with dark proteinaceous organic nodes separating high-Mg calcium carbonate internodes (Noé and Dullo, 2006; Roark et al., 2005). These two components of the coral skeleton grow concentrically and synchronously (Noé and Dullo, 2006), providing temporally linked geochemical records from both organic and calcitic components.

The organic nodes in the bamboo coral skeleton are thought to be derived from particulate organic matter (POM) produced in the surface ocean sinking down to the deep ocean and being captured by bamboo corals through filter feeding (Griffin and Druffel, 1989; Roark et al., 2005). Organic nodes therefore have the potential to record past ocean surface conditions at the time of coral growth. This has been shown using the nitrogen isotopic composition (^{15}N/^{14}N) of the organic nodes to reflect overlying ocean primary

* Corresponding author.
E-mail addresses: qian.liu@bristol.ac.uk, lqian.526@gmail.com (Q. Liu).

https://doi.org/10.1016/j.gca.2023.03.019
0016-7037/

productivity (Hill et al., 2014; Sherwood et al., 2009). Conversely, the calcitic internodes reflect the chemistry of the deeper waters in which the coral grew (Farmer et al., 2015; Hill et al., 2011; Kimball et al., 2014; LaVigne et al., 2011; Roark et al., 2005).

An important component of generating any paleoclimate record is the development of a robust chronology. One of the methods that has been used for developing time-markers in the surface ocean environment is by comparison to the bomb ^{14}C signal (e.g., Campana, 1997; Campana et al., 2008; Frenkel et al., 2017; Roark et al., 2005). Radiocarbon is naturally produced in the atmosphere via cosmic ray interaction with ^{14}N, however unusually large amounts of ^{14}C were produced by atmospheric nuclear tests conducted in late 1950s. The uptake of this bomb ^{14}C by the surface ocean and its subsequent penetration into the deeper ocean not only provides a chronological framework (Scourse et al., 2016; Tisnérat-Laborde et al., 2016), but also enables reconstruction of recent ocean ventilation (Broecker et al., 1978; Druffel, 1989; Lee et al., 2017; Sherwood et al., 2008b). In terms of chronology, bomb ^{14}C is more effectively recorded by surface-ocean archives (e.g., surface-water corals) because of the rapid exchange between surface ocean and the atmosphere (Druffel, 2002; Druffel and Linick, 1978; Fernandez et al., 2015; Hirabayashi et al., 2019; Kilbourne et al., 2007). Two potential time-markers have been suggested – the initial input of ^{14}C around 1957 CE and the time that bomb ^{14}C content reached its maximum (Frenkel et al., 2017; Roark et al., 2005). However, these time-markers are not always straightforward to detect and are dependent on both the resolution of the archive and the synchronicity of these events expressed across the surface ocean (Druffel, 2002; Fernandez et al., 2015; Graven et al., 2012). Ideally, the organic nodes in deep-sea proteinaceous corals would capture both of these ^{14}C time markers to provide an initial chronological framework (Frenkel et al., 2017; Hill et al., 2014; Roark et al., 2006). However, there are problems with synchronicity, and the potential for signals from deeper in the water column to bias the record. Consequently, it is important to develop an alternative independent strategy for chronology development, and in doing so make ^{14}C data a more useful tracer of surface ocean and ventilation processes.

An effective independent method for developing a chronology for bamboo corals is counting of growth bands (visually distinguishable layers of gorgonin (a tough, fibrous protein)) in the organic nodes. Sherwood and Edinger (2009) reported that the organic-node growth bands are annual in two species of bamboo corals (*Keratoisis ornata* and *Acanella arbuscula)* collected off Newfoundland and Labrador. Other deep-sea proteinaceous corals are also thought to form annual bands, presumably in response to the annual cycle in surface-water productivity, e.g., *Primnoa* spp. from the NE Pacific Ocean and NW Atlantic Ocean (Choy et al., 2020; Sherwood et al., 2005a) and black corals (order Antipatharia) from the Gulf of Mexico (Prouty et al., 2011). Annual growth bands of deep-sea proteinaceous organic skeleton could therefore provide a simple and effective approach to develop a detailed chronology of recent live-collected proteinaceous corals (Sherwood et al., 2008b; Williams, 2020). Current evidence points to banding in proteinaceous corals being annual, although further evidence of this in other genera of bamboo corals from other locations would be valuable.

Here we present age model assessments of six bamboo corals collected in 2013 from the central and eastern tropical Atlantic from 700 to 2000 m water depth. We combine chronologies based on band-counting, with ^{14}C and nitrogen isotopic compositions to reassesses the utility of organic node geochemistry for recording surface water processes and provide new records of the ^{14}C in the near surface ocean and thermocline over the last ~150 years.

2. Materials and methods

2.1. Coral samples

Six deep-sea bamboo corals were collected by remotely operated vehicle during the RRS *James Cook* expedition JC094 in October 2013 (Robinson, 2014, Fig. 1, Table 1) from Carter (Car) and Knipovich (Kni) Seamounts (Fig. 1b) and Vema Fracture Zone (Vem) and Vayda (Vay) Seamount (Fig. 1c) in the tropical Atlantic Ocean. We use a simplified sample identifier notation that includes the abbreviated location name and water depth information for each coral sample (e.g., Car_760m for the sample from Cater Seamount at 760 m). All corals in this study were identified as "live" during collection due to the presence of polyp tissue on the skeleton. Polyp tissue was removed from the specimens and the skeletons were preserved dry. All six corals were identified as sub-family Keratoisidinae (Gray, 1870) based on their long and visible (>1 cm) organic nodes (Tracey et al., 2014). Furthermore, they were identified as three different genera according to their branching features: *Lepidisis* (Verrill, 1883) (no branches), *Keratoisis* (Wright, 1889) (branching from the calcitic internodes) and *Acanella* (Gray, 1870) (branching from the organic node). Although France (2007) suggest *Keratoisis* spp. and *Lepidisis* spp. might be the same genus and it may not be appropriate to distinguish by the presence of branching, we still adopt this conventional method of identification.

2.2. Oceanographic Setting

The 700–2000 m depth range where the six bamboo corals were collected is filled by two main water masses: Antarctic Intermediate Water (AAIW) and North Atlantic Deep Water (NADW). Two samples grew in AAIW (Car_760m, Kni_720m), three grew at the boundary of AAIW and NADW (Car_1409m, Vay_1455m and Vem_1474m) and one grew in NADW (Kni_1985m) (Fig. 1d).

The overlying surface/subsurface waters of the central and eastern coral sites are within or along the boundary of a downwelling region and an upwelling region (Fig. 1a), respectively. These differences in oceanographic setting produce different mixed layer (ML) depths and thus different $\Delta^{14}C$ profiles between sites (Fig. 1e). The ML depth in the central tropical Atlantic is ~60 m while in the eastern tropical Atlantic it is shallower at ~30 m (Boyer et al., 2018). Consistent with this vertical mixing pattern, the $\Delta^{14}C$ decreases from west to east as shown by the surface ^{14}C distribution in 1980 CE extracted from Earth System model outputs (see Section 2.4.3) (Fig. 1a).

2.3. Analytical techniques

2.3.1. Sample preparation

An organic node was chosen from near the base of each specimen to capture the longest lifespan of the coral. Additionally, two organic nodes were cut from the middle (node 15: the 15th node from the bottom) and top (tip node) parts of the coral for specimen Vem_1474m and one middle organic node (node 2) for specimen Kni_1985m. Each node was detached from the calcitic internode using a rotary cutting tool. They were then placed into 2 N HCl for 24 h to dissolve any calcite (following Sherwood et al., 2008b). After rinsing with Milli-Q water and drying, the isolated nodes were photographed under a light microscope (Fig. 2). The nodes were subsampled radially at 0.1 to 0.5 mm resolution by peeling away layers using a scalpel blade and tweezers. It was not possible to separate individual gorgonin growth bands, there-

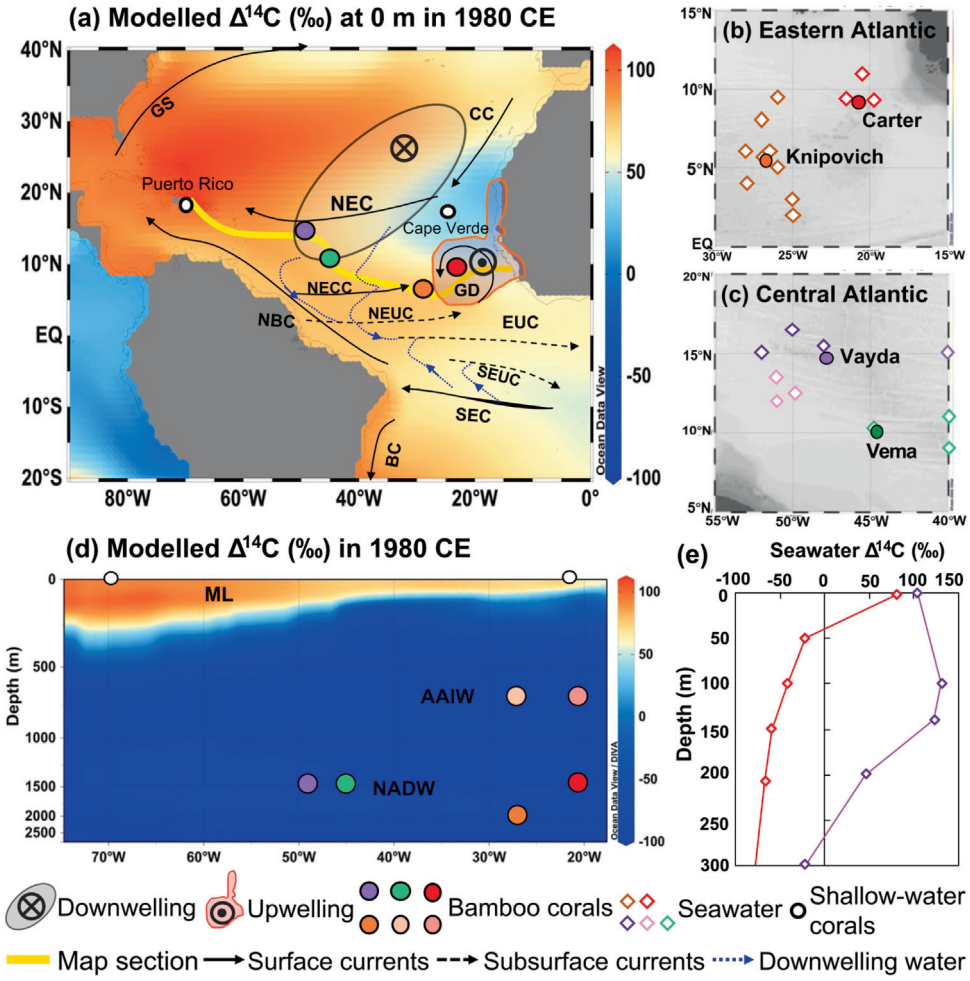

Fig. 1. (a) Locations of bamboo corals in this study (filled symbols) with locations of previously published $\Delta^{14}C$ (age corrected; Eq. (2)) records discussed in the text derived from shallow-water corals (white circles with black edge). The background of this map represents surface $\Delta^{14}C$ of climate model outputs in 1980 CE (see Section 2.4.3). Schematic general circulation patterns are also shown (after (Schott et al., 2004)). The tropical/subtropical downwelling and off-coast upwelling areas of the Atlantic subtropical cells are shown as grey and black boundary with ⊗ and orange boundary with ⊙, respectively. The wide yellow line shows the section location of (d). GS = Gulf Stream; CC = Canary Current; NEC = North Equatorial Current; NECC = North Equatorial Countercurrent; NEUC = North Equatorial Undercurrent; GD = Guinea Dome; EUC = Equatorial Undercurrent; SEUC = South Equatorial Undercurrent; SEC = South Equatorial Current; NBC = North Brazil Current; BC = Brazil Current. (b) Detailed coral locations of eastern Atlantic with seawater $\Delta^{14}C$ sampling locations (open-coloured diamonds). (c) Detailed coral locations of central Atlantic with seawater $\Delta^{14}C$ sampling locations (open-coloured diamonds). (d) Coral depths. Water masses indicated by climate model outputs $\Delta^{14}C$ (Danabasoglu, 2019; Orr et al., 2017). AAIW = Antarctic Intermediate Water; NADW = North Atlantic Deep Water. ML = Mixed Layer. Note that the depth scale is stretched from top. (e) Seawater $\Delta^{14}C$ profiles of 1973 CE in the upper 300 m seawater near the two coral locations to demonstrate the seawater $\Delta^{14}C$ gradient (GEOSECS; Stuiver, 1980). Symbols and their colour are correspondent with figures hereafter unless indicated. (For interpretation of the references to colour in this figure legend, the reader is referred to the web version of this article.)

Table 1
Coral specimens analysed in this study.

Coral name	Coral ID	Genera	Seamount	Depth (m)	Lat (°N)	Lon (°E)	Node radius (mm)	Total growth bands	Average growth rate (μm/yr)	Growth time range
Car_760m	JC094-B0143	*Keratoisis*	Carter	760	9.22	−21.31	1.70	26 ± 6	65 ± 16	1987.8–2013.8
Car_1409m	JC094-B0132	*Acanella*	Carter	1409	9.21	−21.30	6.63	64 ± 8	104 ± 13	1949.8–2013.8
Kni_720m	JC094-B0076	*Keratoisis*	Knipovich	720	5.63	−26.95	1.27	20 ± 1	63 ± 3	1993.8–2013.8
Kni_1985m	JC094-B0086	*Lepidisis*	Knipovich	1985	5.60	−26.97	4.26	71 ± 13	60 ± 11	1919–1988
Vem_1474m	JC094-B0150	*Lepidisis*	Vema Fracture Zone	1474	10.74	−44.58	8.51	161 ± 18	53 ± 6	1831–1992
Vay_1455m	JC094-B0092	*Lepidisis*	Vayda	1455	14.86	−48.24	7.65	114 ± 15	67 ± 9	1898–2013.8

fore subsamples represent multiple years of growth. Only the outer part was sampled for the three additional upper nodes on Vem_1474m and Kni_1985m. Each separated subsample was photographed to count its growth bands, and the diameter was measured at the widest part. Subsamples were again placed into 2 N HCl for 24 h to further dissolve away any residual calcite and dried at room temperature after rinsing with Milli-Q water.

2.3.2. Radiocarbon analysis

Radiocarbon analyses were conducted at the Bristol Radiocarbon Accelerator Mass Spectrometry (BRAMS) Facility at the University of Bristol following the procedure of Knowles et al. (2019). About 2.5 mg of each organic node sample was weighed and burned in the Elemental Analyzer to generate CO_2 to be graphitized in the IonPlus AGE3 graphitization system. IAEA-C7 and OX II

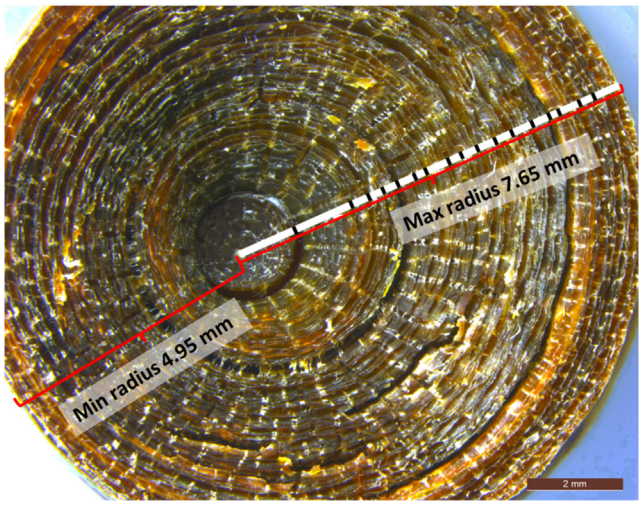

Fig. 2. Example section of Vay_1455m organic node. Markings show individual layers subsampled in preparation.

oxalic acids were used as standards and phthalic anhydride was used as the blank to correct for instrumental background. The graphite targets were analysed by AMS.

The ^{14}C data were originally provided as blank-corrected fraction modern (F_m) which is the $\delta^{13}C$-normalized ratio between the measured sample $^{14}C/^{12}C$ and the $^{14}C/^{12}C$ of NBS Oxalic Acid II at 1950 CE. $D^{14}C$ (‰; age uncorrected) and $\Delta^{14}C$ (‰; age corrected) were calculated using Eqs. (1) and (2) respectively (Stuiver and Polach, 1977):

$$D^{14}C\ \ (‰) = (F_m - 1) * 1000 \quad (1)$$

$$\Delta^{14}C\ \ (‰) = \left[F_m * e^{\lambda(1950-Y_c)} - 1\right] * 1000 \quad (2)$$

where Yc is the coral skeleton formation year derived from the age model calculated in Section 2.3.4 and λ is the reciprocal of the true mean ^{14}C life (8267 years, (Godwin, 1962)). $\Delta^{14}C$ allows direct comparison of ^{14}C content in samples from different ages by accounting for ^{14}C decay occurring between the time of sample formation and ^{14}C analysis.

2.3.3. Nitrogen isotopic compositions ($\delta^{15}N$) analysis

Corals Car_1409m and Vay_1455m were selected for $\delta^{15}N$ measurements because they captured the most complete bomb ^{14}C curve (see Results). The centre, middle and outermost subsamples were measured for both corals. Samples were gently ground to homogenise, weighed out into 0.5–1 mg aliquots into 3.5 × 5 mm tin capsules (part #041060) from Costech Analytical Technologies, Inc and sent out for the $\delta^{15}N$ analyses to the Center for Stable Isotope Biogeochemistry (CSIB), University of California Berkeley. The nitrogen content in the coral organic nodes was 14–16% by weight. The $\delta^{15}N$ values were determined in duplicates in continuous flow mode using a CHNOS Elemental Analyzer (vario ISOTOPE cube, Elementar, Hanau, Germany) coupled with an IsoPrime 100 mass spectrometer (Isoprime Ltd, Cheadle, UK). The N isotope abundance is reported in delta (δ) notation in parts per thousand (‰):

$$\delta^{15}N = ((R_A/R_S) - 1) \times 1000$$

where R_A and R_S are the $^{15}N/^{14}N$ ratios in the sample of interest and in an international standard, respectively. The international standard for $\delta^{15}N$ is atmospheric nitrogen (N_2). Raw instrument data were corrected for drift over time and linearity before normalized to the international stable isotope reference scale. For quality control, NIST (National Institute of Standards and Technology, Gaithersburg, MD, USA) SMR 1577c (bovine liver) previously calibrated against IAEA certified reference materials was used.

The reported long-term precision for $\delta^{15}N$ at CSIB laboratory is 0.2‰. The standard deviation for the sample replicates, run in two different sets on two separate days, was 0.01–0.1‰, except for two samples, Car_1409m Sample No.4 and 9 (Table S1), for which the standard deviation was 0.3‰ and 0.8‰, respectively. The large standard deviations for these two samples were attributed to incomplete homogenization, and likely resulted from natural variability within the chosen bands.

2.3.4. Age model development

Our primary method for the development of the age model for each coral was band counting of the organic nodes. Growth bands within each separated subsample were counted at the widest part of the node, and the total growth bands for each colony were determined as the sum of each individual subsample (Table 1 and Table S1). Counting was independently repeated by one person during three non-consecutive sessions to assess confidence in the result. The average of these three counts was used as the number of growth bands for each subsample. The precision of growth band counting was assessed by using the standard deviation of three different counts of each subsample and averaged ±0.6 bands.

The calendar year for each band was assigned assuming annual banding. The collection date (decimal year 2013.8) was assigned to the coral edge unless there was evidence to suggest that the coral had stopped growing earlier (see Section 4.1.2). We then cross-referenced these ages with the ^{14}C record from the sample coral, and from ^{14}C in nearby seawater and surface water corals from the region. This exercise allowed us to assess whether the coral was growing when it was collected, and to interpolate growth rates where needed (see Supplementary Materials).

2.4. Comparative $\Delta^{14}C$ data compilation

We compiled reported $\Delta^{14}C$ data from the region to provide a comparative basis for our new coral data. These include seawater dissolved inorganic carbon (DIC) data, records from surface-dwelling corals, and from an Earth System Model output (CESM2-FV2-historical model conducted by NCAR; Danabasoglu, 2019).

2.4.1. Seawater DIC $\Delta^{14}C$ data

Thirty-four seawater $\Delta^{14}C$ data points collected from the surface to 150 m depth seawater between 2°N and 11°N, 19°W and 28°W (Fig. 1b) and measured between 1973 CE and 2013 CE were collated for the eastern tropical Atlantic (Table S2; Chen et al., 2015; Kromer, 2014; Olsen et al., 2019, 2020). The seawater $\Delta^{14}C$ ranged from −43.7‰ at 98 m water depth in 1973 CE to 113.8‰ at 23 m water depth in 1983 CE. Data were binned into three groups by depth: 0–29 m, 30–89 m, 90–150 m. The 0–29 m surface layer was based on the average mixed layer depth at the eastern coral site (~30 m; Boyer et al., 2018). Other depth groups were delineated based on available data.

For the central tropical Atlantic, thirty-eight seawater $\Delta^{14}C$ measurements collected from surface to 350 m depth seawater between 7°N and 18°N, 40°W and 54°W (Fig. 1c) and measured between 1957 CE and 2013 CE were included (Table S2; Broecker et al., 1960; Chen et al., 2015; Olsen et al., 2019, 2020). The surface seawater $\Delta^{14}C$ ranged from −73 ± 6‰ in 1957 CE to 136.6‰ in 1973 CE. These data were binned into four groups by depth: 0–59 m, 60–149 m, 150–249 m, 250–350 m. As above, the surface layer (0–59 m) was separated based on the average mixed layer depth at the coral site (~60 m; Boyer et al., 2018), while other depth groups were based on available data.

2.4.2. Shallow-water coral $\Delta^{14}C$ records

$\Delta^{14}C$ records derived from shallow-water corals in Puerto Rico and Cape Verde were compiled to provide continuous surface-water reconstructions. The Puerto Rico $\Delta^{14}C$ record (Kilbourne et al., 2007) is from a location about 2100 km northwest of the central tropical Atlantic coral sites. In the eastern tropical Atlantic two $\Delta^{14}C$ records from Cape Verde provide a shallow-water reconstruction (Druffel, 2002; Fernandez et al., 2015) 900 km north of Carter Seamount and 1300 km north of Knipovich Seamount (Druffel, 2002; Fernandez et al., 2015).

2.4.3. Earth-System-Model-derived $\Delta^{14}C$ records

NCAR Community Earth System Model Version 2 (CESM2-FV2) model outputs of abiotic DIC ('dissicabio') and $DI^{14}C$ ('dissi14cabio') (Danabasoglu, 2019; Orr et al., 2017) were used to calculate predicted seawater $\Delta^{14}C$ using the following equation (Orr et al., 2017):

$$\Delta^{14}C_{ocn}^{abio} = (\text{dissi14cabio}/\text{dissicabio} - 1) \times 1000 \quad (3)$$

for the period 1950 CE to 2014 CE at different depths (0 to 250 m) for each coral location. The predicted seawater $\Delta^{14}C$ of North Atlantic at 0 m in 1980 CE was also calculated (Fig. 1a).

3. Results

3.1. Growth bands and ages

The average number of growth bands for the basal organic node of six specimens range from 20 ± 1 to 161 ± 18 (1SD: standard deviation) (Table 1). The average number of bands within each subsample layer was 6 bands (Table S1). The three replicated counts for each of these sections had an average SD of ± 0.6 bands. Fig. 2 shows an example of the band counting results displayed on the original organic node cross-section.

The lifespans of the six corals range from 20 ± 1 to 161 ± 18 years based on the age model developed by annual band counting of the basal node assuming the banding is annual (Section 2.3.4). Due to the accumulated error propagation, the older section of each coral is expected to have higher uncertainty. The relative SDs of the age estimations range from 5% to 23% with the least precise relative age estimation on the coral Car_760m which is ±6 years over a total lifespan of 26 years (23%). The lifespan time range is listed in Table 1 for each coral together with its average growth rate. The oldest coral Vem_1474m is dated back to 1831 CE with a cessation in growth in year 1992 CE (Table 1). The cessation date for the basal node was assessed by comparing the ^{14}C content of the coral with a record derived from the nearby coral, Vay_1455m (Section 4.1.2).

3.2. Radiocarbon content

The ^{14}C content ($D^{14}C$, not age-corrected) versus distance from coral edge (youngest part) is shown in Fig. 3 for each organic node subsample. $D^{14}C$ recorded in the 9 organic nodes (from 6 corals) range from −71 ± 3‰ to 77 ± 3‰. The two smallest specimens (Car_760m and Kni_720m) exhibit enriched ^{14}C content ($D^{14}C$ values are higher than 50‰) throughout their lifespans (Fig. 3a and c). ^{14}C content recorded in the other four basal nodes are depleted in the centre, becoming more enriched in their outer parts.

For specimen Kni_1985m, the $D^{14}C$ of the outermost layer of node 2 shows a value (70 ± 3‰) equivalent to the outermost layer of the basal node (70 ± 3‰) (Fig. 3d). However, the maximum $D^{14}C$ (77 ± 3‰) recorded in the basal node is not captured in node 2, likely due to the lower sampling resolution within this node. By contrast, for specimen Vem_1474m, the $D^{14}C$ in the outermost layers of the three analysed nodes were markedly different (Fig. 3f), with lower $D^{14}C$ values in upper nodes, i.e., 68 ± 3‰ in the basal node, 62 ± 3‰ in node 15, and 26 ± 3‰ in the tip node.

3.3. Radiocarbon variation over time

The $\Delta^{14}C$ (age-corrected with Eq. (2)) content versus calendar year determined by band counting recorded in the six corals are shown in Fig. 4. The pre-bomb $\Delta^{14}C$ content was constant both in the eastern (−56 ± 3‰) and central (−58 ± 3‰) sites (Fig. 4a and d). In the early 1960 s the $\Delta^{14}C$ increased rapidly (although at different rates) until it reached broad peak values in ~1994 CE (62‰) and ~1980 CE (73‰) for corals Car_1409m and Kni_1985m collected from the eastern Atlantic (Fig. 4a). For the two young corals collected from the eastern Atlantic, with $\Delta^{14}C$ higher than 50‰ throughout their lifespans, $\Delta^{14}C$ generally decreased through time from the beginning of their lifespans, which is 1988 CE for coral Car_760m and 1994 CE for coral Kni_720m (Fig. 4a).

For the central Atlantic, coral Vay_1455m reaches a broad peak $\Delta^{14}C$ at ~1995 CE (69‰) (Fig. 4d). Coral Vem_1474m only has one outermost subsample which captured bomb ^{14}C and the age of this datapoint was estimated by interpolation to the ^{14}C curve of coral Vay_1455m (Fig. 4; Supplementary Materials; Fig. S2).

3.4. Organic node $\delta^{15}N$

The total range of $\delta^{15}N$ recorded in organic nodes is from 8.6‰ to 12.3‰, with a higher average organic node $\delta^{15}N$ recorded in the east Atlantic coral Car_1409m (11.5 ± 1.0‰) than the central Atlantic coral Vay_1455m (9.1 ± 0.3‰) (Table S1; Fig. 5a).

4. Discussion

4.1. Assessing growth rates and annual banding of bamboo corals

We begin with the assumption that the coral genera *Keratoisis*, *Acanella* and *Lepidisis* form annual growth bands in the organic nodes. Only *Keratoisis* and *Acanella* have been examined previously, and both of these genera were reported to have annual banding (Sherwood and Edinger, 2009). We use the associated age models to calculate growth rates for comparison with prior studies. We also use ^{14}C evidence to test the theory that the growth bands apparent in the bamboo corals in our study were formed annually.

4.1.1. Inter- and intra-coral growth rate differences

The average radial growth rate of each bamboo coral ranges from 53 ± 4 μm/yr (Vem_1474m) to 104 ± 10 μm/yr (Car_1409m) (Table 1) which is within the range of growth rate for bamboo corals estimated in previous studies (Table S3; Andrews et al., 2009; Farmer et al., 2015; Frenkel et al., 2017; Hill et al., 2011; Roark et al., 2005; Sherwood and Edinger, 2009; Thresher, 2009; Tracey et al., 2007).

Band-counting age models can also provide more detailed insights into growth rates throughout the coral lifespan (Fig. S2; Table S1). In general, linear growth rates appear to be twice as fast in early central growth before slowing over time towards the outer edge of the coral (Fig. S2; Farmer et al., 2015). This is consistent with the higher growth rates in the centre of the radial section indicated by the trace metal and stable isotope ($\delta^{13}C$ and $\delta^{18}O$) distributions in the calcitic internodes of bamboo corals (Flöter et al., 2019; Sinclair et al., 2011).

The growth rates of bamboo corals have previously been compared with the ambient environment to identify any potential external controls on growth (Farmer et al., 2015; Thresher, 2009; Thresher et al., 2016). Obviously, this approach is not

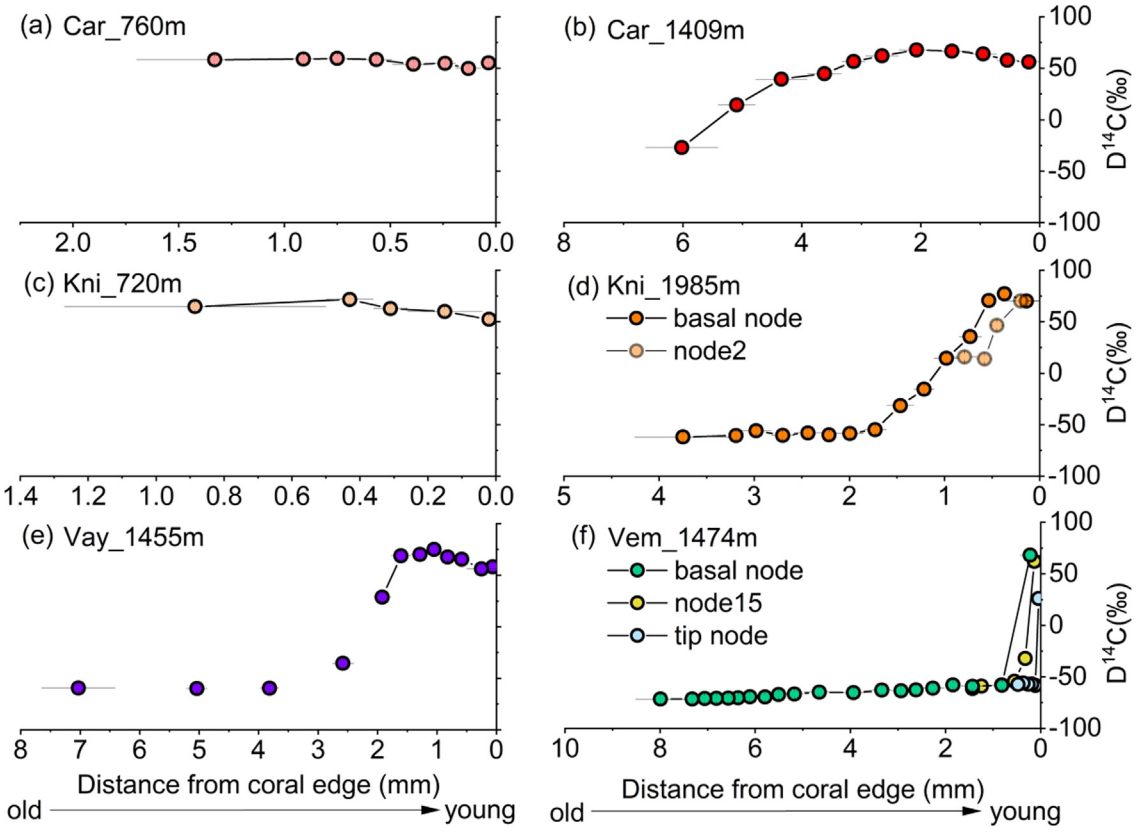

Fig. 3. $D^{14}C$ (no age-correction) versus distance from coral edge (youngest part). X error bar represents the thickness of subsample. Subsamples measured in Vay_1455m are not continuous. Y error bar represents analytical error of $D^{14}C$ and is smaller than symbols.

straightforward for corals which exhibit a non-linear growth rate that is negatively correlated with coral size (Frenkel et al., 2017). Nonetheless, Thresher (2009) and Thresher et al. (2016) concluded that growth rate has a positive correlation with ambient temperature within the most sampled subfamily Keratoisididae (Thresher, 2009; Thresher et al., 2016). By contrast, Farmer et al. (2015) found no significant correlation. Our compiled average growth rate data (Table S3) are in general agreement with Thresher et al. (2016) and show a positive linear correlation ($p < 0.01$; IBM SPSS) between growth rate and ambient temperature (we note that only growth rate data derived from organic nodes have been compiled to minimize the uncertainty stemming from different methods used for growth rate determination). However, when we focus on individual genera among Isididae, the correlation is less clear. *Lepidisis* and *Keratoisis* are two genera that have been relatively well studied and show significant ($p < 0.05$; IBM SPSS) and weak positive correlation ($p < 0.1$; IBM SPSS), respectively, with temperature. By contrast, *Isidella* shows no significant correlation and higher growth rates than the other two genera. The genus *Acanella* has been less well studied, such that a genus specific correction could not be generated. Thus, the factors that influence the growth of bamboo corals remain unknown despite the increasing amount of data availability. Phylogeny, ambient temperature, and food supply are likely to work together to influence the growth of bamboo corals (Thresher, 2009; Thresher et al., 2016).

A further challenge to the interpretation of growth rate is the asymmetric growth (e.g., off axis centring of earliest growth bands shown in Fig. 2). The maximum radius of the basal organic node of coral Vay_1455m is 7.65 mm while the minimum is 4.95 mm (~35% different). In this study we used the largest radius for consistency between corals. However, if different parts of the radius were measured in previous studies, the correlation between compiled growth rates and ambient temperature would introduce scattering, e.g., 35%, distorting the results.

4.1.2. Testing the band-counting age model

An alternative way to assess growth rate would have been to use the ^{14}C profile of the nodes as compared to the expected ML water value to develop an age model (e.g., Frenkel et al., 2017; Roark et al., 2005), which relies on assumptions about the source of the organic matter within the nodes (i.e., that it reflects the ML). We make a detailed assessment of the age models that would have been acquired by using bomb ^{14}C time-markers (Supplementary Materials; Fig. S2). Our study adds further evidence that growth bands in organic nodes are formed annually and provides additional confidence for the results of both dating techniques. We find the ^{14}C-derived age model and associated growth rate estimates are consistent with band counting with one exception of a single three time-marker chronology developed for Vay_1455m (Fig. S2; Supplementary Materials). Henceforth we use the more precise band-counting age models that permit further investigation of the ^{14}C signal independent of age model development.

We also compare the ^{14}C content of the outermost part of the nodes to modern seawater to test whether each coral was still growing when it was collected. Based on this comparison, all corals except Kni_1985m and Vem_1474m were found to be still growing on collection. By contrast, coral Kni_1985m showed about 20‰ offset between the coral edge and both the overlying ML and upper thermocline seawater (0–55 m) $\Delta^{14}C$ in 2013 (Fig. 4a). The organic node $\Delta^{14}C$ of coral Vem_1474m never reached the bomb ^{14}C peak, potentially implying a long (more than a decade) cessation in growth preceding collection (Fig. 4d). To check if the growth

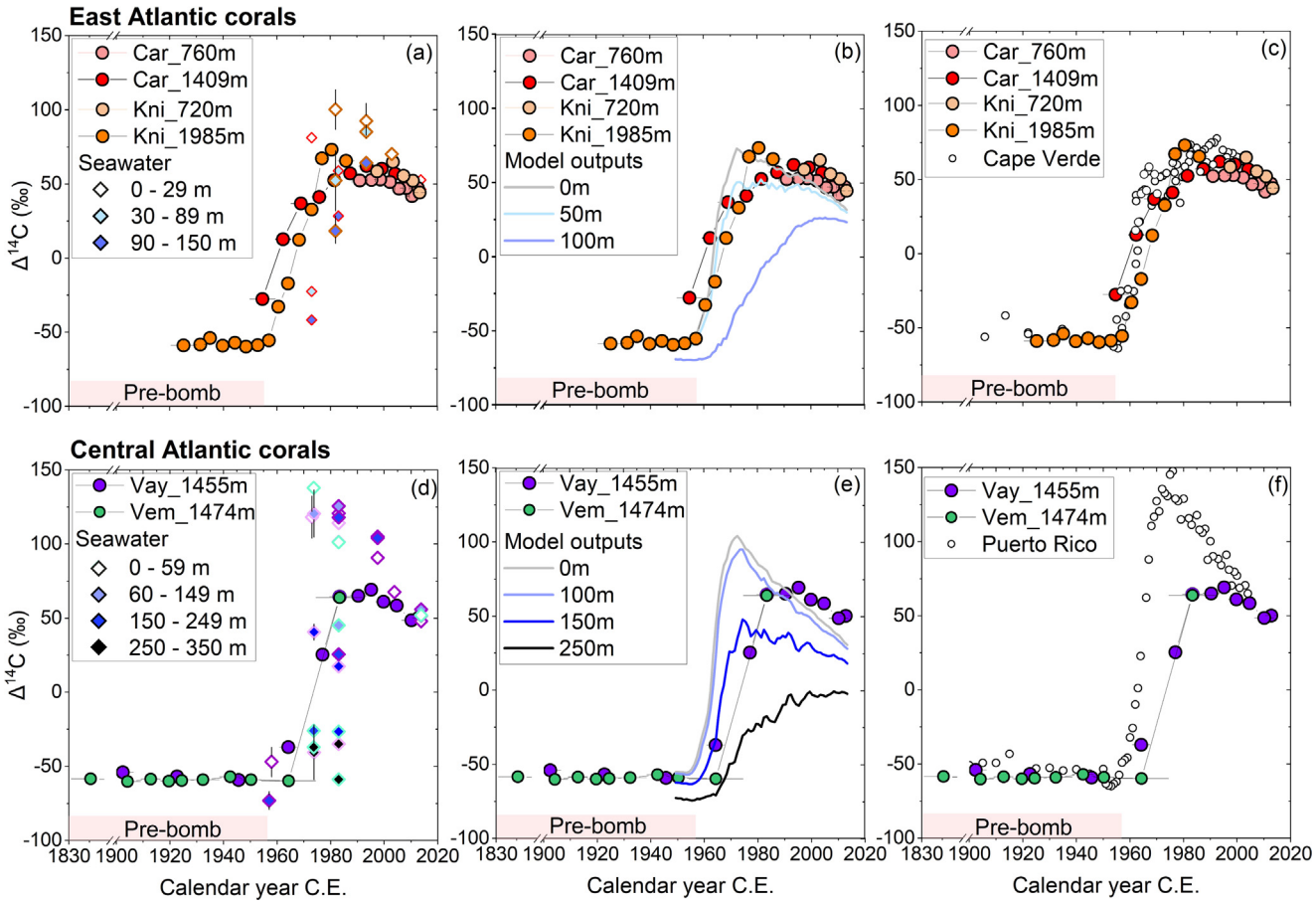

Fig. 4. $\Delta^{14}C$ (age-corrected) recorded in organic nodes of six bamboo corals in eastern (a–c) and central (d–f) tropical Atlantic compared with observed seawater $\Delta^{14}C$ (a, d), seawater $\Delta^{14}C$ derived from CESM2 model outputs (b, e) and $\Delta^{14}C$ recorded in shallow water coral (c, f). Coloured circles with black borders refer to bamboo corals. Diamonds refer to observed seawater dissolved inorganic carbon (DIC) average $\Delta^{14}C$ at different depth intervals as indicated by filled colour. The colours of diamonds borders refer to the location of seawater shown in Fig. 1(b) and (c). The Y-error bar represents the variation range of seawater $\Delta^{14}C$ in the locations indicated by the same colour shown in Fig. 1(b) and (c). Seawater data are from GLODAPv2.2020) (Olsen et al., 2019; Olsen et al., 2020; Stuiver, 1980). The lines refer to model outputs $\Delta^{14}C$ at depths indicated by colour (historical experiment of CESM2-FV2 model conducted by NCAR (Danabasoglu, 2019)). Model outputs are extracted from Carter Seamount and Vayda Seamount overlying upper layers, respectively. White circles refer to shallow-water coral records in Cape Verde Island (Druffel, 2002; Fernandez et al., 2015) for the eastern site (c) and in Puerto Rico (Kilbourne et al., 2007) for the central site (f). X-error bar represents year range of each subsample.

cessation occurred only in the basal node or the entire coral, the outer part of an additional node (node 2: the second node from the bottom) of Kni_1985m and two further nodes (node 15: the 15th node from bottom; and the tip node) were also measured for ^{14}C. $D^{14}C$ was indistinguishable between the outermost nodes of subsamples of Kni_1985m, which suggests growth of Kni_1985m ceased along the entire coral (Fig. 3d). For Vem_1474m, the $D^{14}C$ of the outermost subsample of the basal node and node 15 show no difference, while $D^{14}C$ of the outermost subsample of tip node was significantly lower, indicating that the cessation in growth likely occurred from the top of the coral (Fig. 3f). The presence of the −32‰ $D^{14}C$ data point in node 15 of Vem_1474m suggests the outermost bomb-influenced subsample grew continuously instead of regrowing after a cessation in growth (Fig. 3f). Previous studies have also reported that the outer part of organic nodes of some bamboo corals did not capture the whole bomb ^{14}C record up to the collection date, even with tissue present on the specimen when collected (Farmer et al., 2015; Frenkel et al., 2017; Hill et al., 2014). Caution must therefore be exercised when using the collection date as a time-marker to construct age models of bamboo corals. In this study, where the ^{14}C record provides evidence that a coral was no longer growing at the date of collection (i.e., Vem_1474m and Kni_1985m), an additional chronological constraint was employed. We assumed that nearby coral would share a common carbon source with the coral that ceased growing and, therefore, the overlapping ^{14}C variation recorded in the organic nodes of Vay_1455m and Car_1409m were used to chronologically constrain Vem_1474m and Kni_1985m, respectively (Fig. 4). Critically, since the ^{14}C record for Vem_1474m and Kni_1985m are not independent of the age model developed for these specimens, any discussion of the timing of ^{14}C signals henceforth focuses only on the annual band-dated Vay_1455m and Car_1409m records.

4.2. Source of ^{14}C recorded in bamboo corals organic nodes

Bomb ^{14}C was found in the organic nodes of all six bamboo corals (Fig. 4). This result provides robust evidence that the carbon source of organic nodes is derived from export of recent organic material (Roark et al., 2005). Importantly however, we note that coral $\Delta^{14}C$ does not always follow the surface ML waters (Fig. 4). The magnitude of the deviation from the ML seawater $\Delta^{14}C$ is smaller in the eastern tropical Atlantic upwelling zone than the central tropical Atlantic subtropical downwelling regime. We therefore separate the discussion in the following sections to consider the two different oceanographic settings and comparative $\Delta^{14}C$ records. By 2013 (the date of sampling) the seawater $\Delta^{14}C$ values within the ML and the upper thermocline were converging

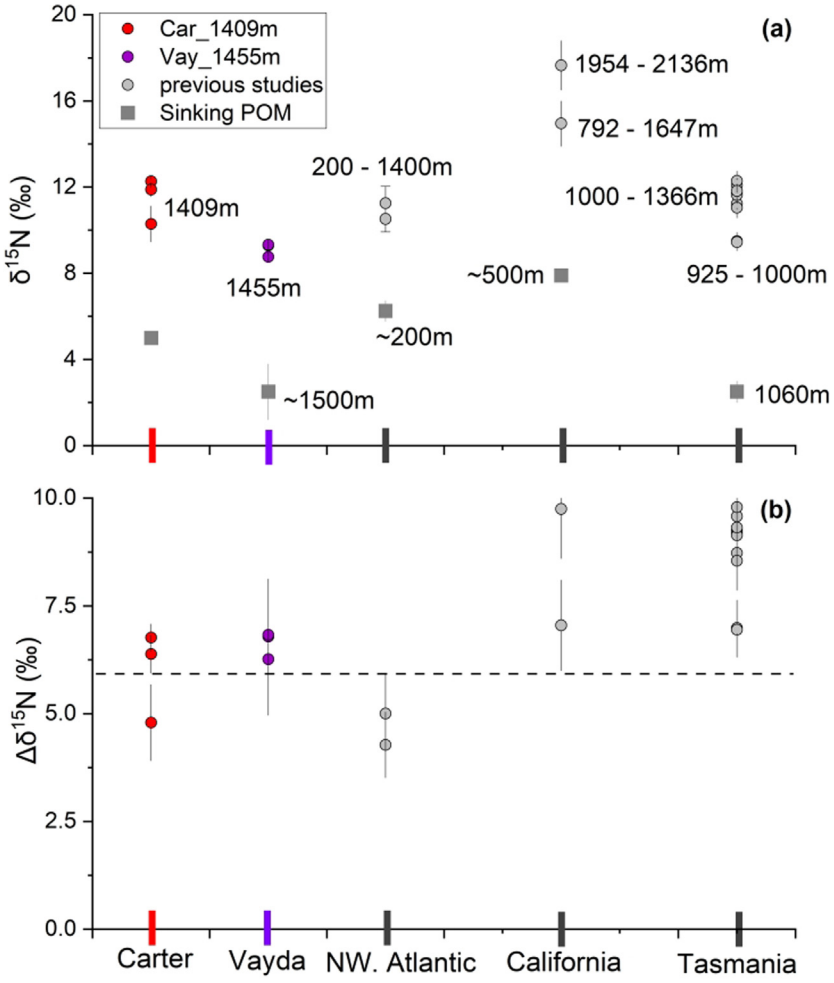

Fig. 5. (a) $\delta^{15}N$ of organic node of bamboo corals in this study and previous studies and nearby sinking POM. (b) $\delta^{15}N$ offset ($\Delta\delta^{15}N$) between bamboo corals and sinking POM of corresponding locations. The text alongside data points in POM $\delta^{15}N$ are the depths of each sediment trap. POM $\delta^{15}N$ of Carter seamount is calculated by stoichiometric method by Marconi et al. (2019).

after the initial invasion of bomb ^{14}C (Fig. 4a and d). Given this convergence it becomes more difficult to separate signals derived from the ML or upper thermocline in more recent times.

4.2.1. Eastern tropical Atlantic

The $\Delta^{14}C$ of the organic node of corals from the eastern sites typically reflect the $\Delta^{14}C$ of seawater from between 0 and 50 m water depth, or slightly deeper at Knipovich (Fig. 4a). This observation is supported by the outputs from CESM2, which shows that seawater $\Delta^{14}C$ values between 0 and 50 m seawater were in agreement with the $\Delta^{14}C$ of the organic node (Fig. 4b).

With the lack of continuous seawater observations and no available seawater $\Delta^{14}C$ observations from this region before 1970, the initial response to bomb ^{14}C and peak times cannot be assessed directly, however shallow-water coral records offer an alternative continuous record for comparison. The closest records are from two shallow-water scleractinian corals from Cape Verde (Druffel, 1996; Fernandez et al., 2015). Interestingly, the Cape Verde records are also slightly offset from ML water $\Delta^{14}C$, although this is likely due to the more south-westerly and offshore positions of seawater sampling locations compared to Cape Verde, with a lower impact of upwelled ^{14}C-depleted water (Grodsky et al., 2008; Schott et al., 2004) and thus higher $\Delta^{14}C$ in the offshore ML waters compared to Cape Verde (Fig. 1a).

The $\Delta^{14}C$ curves recorded in the bamboo corals are very similar to the Cape Verde shallow-water corals, including timings of the initial rise, and the general amplitude of $\Delta^{14}C$ (Fig. 4c) although there are some subtle differences observed in Kni_1985m. The overall agreement between the corals from Cape Verde and the bamboo corals suggests a similar source of carbon across the region and for all corals.

4.2.2. Central tropical Atlantic

In contrast to the eastern sites, in the central tropical Atlantic, we observe a large difference between $\Delta^{14}C$ in ML seawater and bamboo coral organic nodes between 1970 CE and 2000 CE. For example, the ^{14}C content between 1970 CE and 2000 CE in coral Vay_1455m is depleted by up to 110‰ relative to ML seawater $\Delta^{14}C$ from nearby locations (0 m to ~60 m; Boyer et al., 2018) (Fig. 4d). In fact, the organic node $\Delta^{14}C$ curve falls closer to seawater DIC values and model outputs from 150 m to 249 m (Fig. 4d, e). After 2000 CE, the $\Delta^{14}C$ of ML seawater and upper thermocline started to converge, thus we observe organic node $\Delta^{14}C$ values similar to ML seawater $\Delta^{14}C$.

The comparison of $\Delta^{14}C$ records between organic node and shallow-water coral is also different from the eastern sites, with significantly lower $\Delta^{14}C$ in bamboo coral organic nodes than the shallow-water coral from Puerto Rico between the 1970 CE and 2000 CE bomb period (Fig. 4f, (Kilbourne et al., 2007)). In terms

of timing, coral Vay_1455m reaches a broad peak $\Delta^{14}C$ between 1983 CE and 1995 CE, lagging the Puerto Rico shallow-water coral record by 10 to 20 years (Fig. 4f) and with a peak value ~80‰ lower in amplitude. Considering the uncertainty of the age model of coral Vay_1455m, which is ~5 years between the broad peak period (Table S1), the lower amplitude and time lag is robust. Further, if the age model was instead forced so that the maximum ^{14}C bomb peak in Vay_1455m was aligned to the Puerto Rico shallow water coral, the generated growth rates would shift unrealistically to become extremely slow for the last 40 years of the coral's life (Supplementary Materials, Fig. S2). This apparent artefact in growth is not evident in the other age models investigated, whether band-counting or ^{14}C-based (Supplementary Materials). Alternatively, the consistent depleted and lagged $\Delta^{14}C$ in organic nodes compared to both ML seawater and shallow-water coral suggests a different carbon source for the bamboo corals in this region. We consider three possible scenarios: (1) different oceanographic settings between arising due to the spatial separation the bamboo corals and shallow-water coral in Puerto Rico; (2) degraded/aged POM being incorporated in organic nodes; (3) organic nodes recording thermocline seawater $\Delta^{14}C$ instead of ML $\Delta^{14}C$. The evidence outlined below suggests that the third scenario is the most likely cause.

The oceanographic settings between the bamboo corals obtained from open ocean seamounts and shallow water Puerto Rico coral are indeed different. Puerto Rico is located to the northwest, within the Caribbean Sea (Fig. 1a). The surface water masses influencing the Puerto Rico site are a combination of the southern-sourced, ^{14}C-enriched North Brazil Current and the northern-sourced North Equatorial Current (NEC) (Hernández-Guerra et al., 2005). However, surface waters around Vayda Seamount are mainly derived from the NEC. Source water differences between Puerto Rico and Vayda Seamount could lead to different bomb ^{14}C evolution. Although we do not have a time-resolved $\Delta^{14}C$ record for the NEC (more tropical Atlantic coral ^{14}C records are required), a difference in source waters between Puerto Rico and Vayda Seamount is indicated by the model outputs shown in Fig. 1a. The general surface ^{14}C distribution in 1980 CE suggests higher $\Delta^{14}C$ in the ML water of Puerto Rico than in the Vayda Seamount. However, the difference is only 20‰ for the bomb $\Delta^{14}C$ peak in the two locations, which accounts for only a portion of the ~80‰ depletion in the organic node ^{14}C peak. Therefore, although the difference in the oceanographic settings between locations must contribute in part to the observed difference, it cannot fully explain the ^{14}C depletion observed in the Vayda Seamount bamboo coral organic nodes.

Degraded/aged POM is ^{14}C depleted and would therefore lead to lower $\Delta^{14}C$ if incorporated in organic nodes. Sherwood et al. (2009) hypothesized degraded/aged POM as food source of bamboo corals to explain the high $\delta^{15}N$ observed in the coral organic nodes. Although our $\delta^{15}N$ cannot entirely exclude this possibility (Section 4.3), the ^{14}C evidence suggests this scenario is less likely. Although a depleted and lagged peak $\Delta^{14}C$ is recorded in the organic node, there is no significant delay observed in the $\Delta^{14}C$ of corals from either eastern and central site, for the initial response to bomb ^{14}C relative to shallow-water corals and modelled $\Delta^{14}C$ records (Fig. 4), which would be expected if degraded, and thus older, suspended POM were the primary dietary source. In addition, previous studies showed large $\Delta^{14}C$ (−400‰) gradients in suspended (degraded/aged) POM between upper water column and coral growth depths (~1450 m) (Bauer et al., 2001; Bauer et al., 2002), which if incorporated would result in lower $\Delta^{14}C$ in the organic node. Two observations however suggest that degraded POM incorporation is unlikely: (i) the $\Delta^{14}C$ recorded in organic node is indistinguishable from ML seawater since the 2000 s due to the upper water $\Delta^{14}C$ converging (Fig. 4d, e) and (ii) there is a close fit between pre-bomb organic node $\Delta^{14}C$ and modelled $\Delta^{14}C$ in the ML (Fig. 4e).

After excluding the first two scenarios, we hypothesize that the most plausible scenario is that the organic node of bamboo coral in the central tropical Atlantic is recording upper thermocline seawater $\Delta^{14}C$ instead of ML $\Delta^{14}C$. The comparison between organic node and seawater $\Delta^{14}C$ indeed shows that the organic node $\Delta^{14}C$ is more similar to 150 to 250 m (upper thermocline) seawater $\Delta^{14}C$ (Fig. 4d). We note that the organic node $\Delta^{14}C$ does not always follow the 150 to 250 m seawater $\Delta^{14}C$. This could be due to the observed seawater transient variability, or the depth of organic node carbon source changing over the lifespan of the corals. Below we explore the potential mechanism for organic node incorporation of upper thermocline seawater $\Delta^{14}C$.

4.3. How do the organic nodes of bamboo coral record upper thermocline ^{14}C?

The presence of bomb ^{14}C in the outer layers of organic nodes of bamboo corals prompted previous studies to assume that this carbon was derived from surface POM (Roark et al., 2005). However, we interpret the low absolute $\Delta^{14}C$ values and the delayed timing of the maximum in the central tropical Atlantic (Fig. 4d, e, f) as the influence of carbon from below the ML ocean being captured within the organic nodes (Section 4.2.2).

To further investigate the mechanisms behind this carbon acquisition and the trophic transformations, we measured the $\delta^{15}N$ of the organic nodes of bamboo corals from the eastern and central tropical Atlantic. The average $\delta^{15}N$ for the eastern tropical Atlantic is 11.5 ± 1.0‰. Thus, the offset ($\Delta\delta^{15}N$) between the organic node and the likely $\delta^{15}N$ of POM (~5.5‰ as estimated by Marconi et al. (2019) using a stoichiometric method) averages 6.0 ± 1.0‰ for corals collected from the eastern tropical Atlantic Ocean (Fig. 5b). For the central site, the average organic node $\delta^{15}N$ is 9.1 ± 0.3‰. The closest location of previously characterized $\delta^{15}N$ of sinking POM is near Bermuda, where the $\delta^{15}N$ of sediment trap POM at ~1500 m is about 2.5 ± 1.3‰ (Altabet et al., 1991). Thus, for the central tropical Atlantic corals at the Vayda Seamount, we find a similar $\Delta\delta^{15}N$ to the eastern site of ~6.6 ± 1.3‰. The 2.5‰ difference in $\delta^{15}N$ of POM between the eastern and central Atlantic sites is consistent with differing nitrogen sources supporting primary production. The source of nitrogen for the phytoplankton in the eastern Atlantic is deep thermocline nitrate with a $\delta^{15}N$ of ~5.5‰ (Marconi et al., 2015). In the central Atlantic, the $\delta^{15}N$ of the thermocline nitrate is 2-3‰, reflecting a mixing signal between deep nitrate of ~5‰ and a contribution from biological N_2 fixation of ~0‰ (Marconi et al., 2015). The difference in the $\delta^{15}N$ of the nitrogen supporting primary production appears to be transferred to the $\delta^{15}N$ of the organic nodes, with no apparent difference in trophic transformations across the food web from phytoplankton to coral feeding, in other words, with a relatively constant $\Delta\delta^{15}N$.

The magnitude of $\Delta\delta^{15}N$ reported here broadly agrees with those found in bamboo corals collected from other locations at intermediate depths (792–1647 m) of the California margin (Hill et al., 2014), Labrador continental margin (Sherwood et al., 2008a) and Tasmanian margin (Sherwood et al., 2009) (Fig. 5b). However, larger $\Delta\delta^{15}N$ values were observed from deeper (1954–2136 m) corals on the Californian margin (Hill et al., 2014) and *Lepidisis* spp. collected from 1000 to 1366 m depths on the Tasmanian margin (Sherwood et al., 2009), which were interpreted as degraded POM being consumed by deeper corals. By comparison, an ~8–9‰ $\Delta\delta^{15}N$ between primary production and coral organic matter has been reported for deep-sea scleractinian corals (e.g., *Desmophyllum dianthus*), which has been interpreted as a larger contribution of degraded suspended POM to the scleractinian coral diet (Wang et al., 2014).

Assuming that the average $\delta^{15}N$ isotope effect per trophic level is about 3‰ (e.g., food web studies (Deniro and Epstein, 1981; Macko et al., 1982)), then 2 trophic transfers would account for the ~6‰ $\delta^{15}N$ offset. To explain this offset, we can invoke two possible dietary sources: (1) degraded suspended POM; (2) zooplankton which have consumed fresh POM.

Degraded suspended POM $\delta^{15}N$ is typically ~3–4‰ higher than fresh sinking POM (Altabet, 1988; Saino and Hattori, 1987). Although degraded POM would fit well with our $\delta^{15}N$ data, we can exclude this possibility based on our discussion of $\Delta^{14}C$ in Section 4.2.2. In addition, $\Delta^{14}C$ data recorded in bamboo corals from different depths show no significant difference as would be expected for degraded POM (Car_760m and Car_1409m; Fig. 4a–c). The comparable $\Delta\delta^{15}N$ between eastern and central bamboo corals provides further evidence that degraded POM is unlikely to be the primary food source of bamboo corals, otherwise $\Delta^{14}C$ in the organic nodes would be more depleted than ML seawater and Cape Verde shallow-water corals, which is not observed in the eastern bamboo corals (Fig. 4a, c).

An alternative dietary source is zooplankton, as suggested by both Sherwood et al. (2009) and Hill et al. (2014). Zooplankton are 1–1.5 trophic levels above phytoplankton, thus with a $\delta^{15}N$ of 3–5‰ higher than fresh sinking POM (Koppelmann et al., 2009). Combined with the additional trophic level of corals, a diet of zooplankton for bamboo corals would result in $\Delta\delta^{15}N$ from 6‰ to 8‰, providing a plausible fit for the data from both the eastern and central tropical Atlantic bamboo corals. The size of zooplankton has been found to positively correlate with their $\delta^{15}N$ (Kozak et al., 2020; Montoya et al., 2002; Romero-Romero et al., 2020). The average diameter of polyps of bamboo corals is 3–5 mm (Sherwood et al., 2008a), large enough for them to capture sinking (dead) or living migrating or ambient (micro)zooplankton. Indeed, sinking zooplankton have been reported to contribute to the diet of other deep-sea octocorals in Antarctica by feeding experiments (Orejas et al., 2003). Therefore, a combined diet of sinking phytoplankton and zooplankton is likely the best explanation for the $\delta^{15}N$ and $\Delta^{14}C$ values of bamboo corals collected from both eastern and central sites.

The upper thermocline habitat (i.e., below the ML) of the phytoplankton that serve as the base trophic level in the diet of bamboo corals would explain how the organic nodes of bamboo corals incorporate upper thermocline $\Delta^{14}C$. In oligotrophic regions (e.g., central Atlantic; Fig. 1a), the highest abundance of phytoplankton is found within the deep chlorophyll maximum (DCM) (Latasa et al., 2017), typically located near the base of the euphotic zone (Claustre and Marty, 1995). The position of DCM can occur below the ML (Ellwood et al., 2018), especially in the oligotrophic subtropical regions. Thus, a significant portion of phytoplankton could live and support zooplankton below the surface ML. For instance, a study in the South Pacific subtropical gyre found up to 90% of net community exported production, likely available to zooplankton, is generated below the ML, at 80–100 m depth (Haskell et al., 2016), or even at ~130 m (Bender and Jönsson, 2016). In addition, a maximum accumulation of POM at the depth of ~160 m was reported in the Pacific subtropical gyre (Claustre et al., 2008). The DCM depth of the central tropical Atlantic is around 150 m with chlorophyll extending to ~200 m (Estrada et al., 2016), more than 100 m below the average ML of that area (~60 m; Boyer et al., 2018). Exported (net) primary production in the central Atlantic therefore incorporate DIC (and thus ^{14}C) from less ventilated waters below ML (upper thermocline) rather than the ML DIC (Fig. 6a). Therefore, the $\Delta^{14}C$ recorded in organic nodes of bamboo corals (from phytoplankton and zooplankton) will be lower than ML seawater $\Delta^{14}C$ (Fig. 6).

By contrast, the eastern sites are in the upwelling region with high nutrients in the ML, supporting relatively high productivity within ML and down to a depth of ~60 m (Agustí and Duarte, 1999; Bode et al., 2015), which is slightly deeper than the ML depth of ~30 m (Boyer et al., 2018). The higher productivity in the ML than in the thermocline in the eastern Atlantic leads to smaller contribution of the deeper carbon (^{14}C depleted) to the POM than at the central sites, leading to similar organic node $\Delta^{14}C$ to ML seawater and shallow-water coral in the eastern sites (Fig. 4a, c; Fig. 6b).

4.4. Implications for using deep-sea proteinaceous corals as palaeoarchives

The organic node of bamboo corals records information delivered with POM (e.g., ^{14}C transfer through trophic levels) from different water depths and is dependent on the oceanographic setting. Previous studies on other deep-sea proteinaceous corals (e.g., *Primnoa* spp.) showed that the carbon source of organic skeleton is derived from recently exported POM (Sherwood et al., 2005b; Williams, 2020). Unlike our coral records from the central tropical Atlantic, previous deep-sea proteinaceous-coral studies reported that surface ML seawater $\Delta^{14}C$ was recorded in the organic skeleton (Hill et al., 2014; Sherwood et al., 2009; Sherwood et al., 2008b). The differences between the sites may well be due to the relative depths of the DCM and the ML. Potential scenarios of the relationships between DCM and ML depths, and the resulting influence on the organic skeleton recorded $\Delta^{14}C$ time-series are demonstrated in Fig. 6.

When there is a DCM below the ML (i.e., a large portion of net community production produced below ML), such as at our central coral sites, the $\Delta^{14}C$ recorded in the organic nodes will be more depleted relative to ML seawater $\Delta^{14}C$ (Fig. 4d; Fig. 6a and d). Depending on the ^{14}C depth profile, larger vertical offsets between ML and DCM depths, as expected for the more oligotrophic central tropical Atlantic, will lead to more depleted $\Delta^{14}C$ recorded in organic node at these sites because of the steep decrease of $\Delta^{14}C$ below ML (Fig. 6a). This is likely the reason that the organic node $\Delta^{14}C$ records from central sites are more attenuated and delayed compared to surface seawater than those at eastern sites (Fig. 4).

When there is not a pronounced DCM below the ML or the majority of net community production is produced within the ML, such as Monterey Canyon in the California margin where bamboo corals collected from (Hill et al., 2014), the organic skeleton $\Delta^{14}C$ shows no offset from surface ML seawater. Monterey Canyon is a upwelling-dominated, nutrient-replete region where the majority of the net community production is only limited within the ML (~10 m in a closer offshore; Ryan et al., 2005). With the majority of phytoplankton growing within the ML therefore supporting zooplankton, the $\Delta^{14}C$ recorded in the organic node through trophic transfer would show no significant offset from ML $\Delta^{14}C$ (Fig. 6b, d). The organic node $\Delta^{14}C$ recorded in a bamboo coral collected from 714 m from the southwest Grand Banks could also be explained by a similarly shallow depth of phytoplankton growth (Sherwood et al., 2008b). The ML depth in this case is similar to our eastern coral sites (~30 m; Boyer et al., 2018) and the net community production is also only limited within ~30 m (Glover et al., 1986). There could be fluctuations in the depths of DCM and ML when the two depths are close and therefore the organic node $\Delta^{14}C$ could be different from surface ML seawater (Fig. 6b). However, the growth rate of the proteinaceous corals is too slow to resolve the difference in $\Delta^{14}C$ between ML and DCM depth seawater.

Another scenario is that the ML is much deeper than phytoplankton growth depth (Fig. 6c). For example, in the case of the *Primnoa resedaeformis* collected from Hudson Strait (polar North East Atlantic; Sherwood et al. 2008a), there is a thick ML which is relatively homogenous with respect to $\Delta^{14}C$ due to deep winter

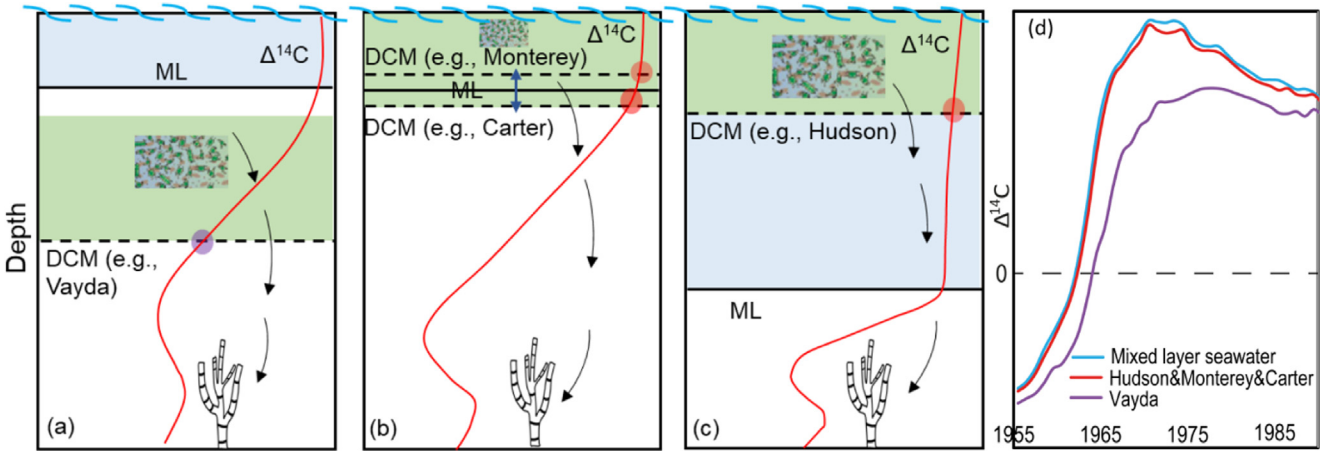

Fig. 6. (a–c) Schematic of three scenarios of the relationship between mixed layer (ML) depth (solid black horizontal lines), the deep chlorophyll maximum (DCM) depth (dashed black horizontal lines) and its influence on $\Delta^{14}C$ recorded in the organic node of deep-sea proteinaceous corals. Blue and green shadings represent simplified schematic ML and phytoplankton layer, respectively. The red curves in (a–c) represent the schematic seawater DIC $\Delta^{14}C$ profiles, respectively. The purple and red dots in (a–c) represent the $\Delta^{14}C$ recorded in organic nodes under different scenarios (colours are matched to d). The double-headed arrow in (b) represents the potential fluctuation between DCM and ML depths. (d) Simplified schematic $\Delta^{14}C$ time-series profiles. (For interpretation of the references to colour in this figure legend, the reader is referred to the web version of this article.)

mixing (e.g., Fig. 6c), thus removing attenuation or delay of bomb ^{14}C influence compared to surface ML seawater (e.g., Sherwood et al., 2008b). The ML depth of Hudson Strait deepens to ~1500 m during the winter and can still be as deep as 100 m in summer (Azetsu-Scott et al., 2005). Therefore, the ^{14}C composition recorded in the organic node will have the same value regardless of the depth that the dietary source of coral originated from. The $\Delta^{14}C$ recorded in calcite from the same coral is identical to the organic skeleton $\Delta^{14}C$ during the pre-bomb period and is not significantly attenuated during the peak bomb time. Given that the calcite portion of the skeleton is thought to document the $\Delta^{14}C$ of ~400 m seawater where the coral grew, this provides further evidence that the ML is sufficiently thick that the subsurface $\Delta^{14}C$ is the same as surface. Another example is from bamboo corals collected from the southeast Tasmanian margin, which is a fairly nutrient-rich regime (Sherwood et al., 2009). Here, the average ML depth is also relatively deep, ranging from 150 to 300 m (Boyer et al., 2018) while the high rates of net community production is limited to within ~50 m (Ellwood et al., 2018) which is much shallower than the ML depth, leading to the organic node recording $\Delta^{14}C$ that is the same as surface ML water $\Delta^{14}C$.

Depending on the relationships between DCM and ML depths, the $\Delta^{14}C$ time-series recorded in the organic skeleton of deep-sea proteinaceous coral will capture different signals as demonstrated in Fig. 6d. Therefore, age models developed by bomb-^{14}C maximum time-markers could be inappropriate in locations where there is a DCM much below the ML (Fig. 6a), with consequence of overestimating average growth rates, thus, could underestimate the lifespans of the corals (e.g., Fig. S2c and g).

5. Conclusions

We show that layers of the organic node of three genera of bamboo corals (*Lepidisis, Keratoisis* and *Acanella*) are formed annually. Six deep-sea bamboo corals have been dated using band-counting and assessed by ^{14}C. Through comparison with existing $\Delta^{14}C$ data, including measured seawater DIC and nearby shallow-water coral records as well as Earth System Model outputs, we interpret organic node $\Delta^{14}C$ to reflect $\Delta^{14}C$ at the depth of maximum rates of net community production. In the oligotrophic waters like the central tropical Atlantic, the $\Delta^{14}C$ of organic nodes reflects that of POM produced within the DCM layer rather than within the ML. Complementary $\delta^{15}N$ data combined with $\Delta^{14}C$ suggest bamboo corals feed mostly on zooplankton, perhaps with some contribution from sinking POM. Through the comparison between ML and DCM depths, we show that the depth interval of $\Delta^{14}C$ recorded in the organic skeleton of deep-sea proteinaceous corals depends on the overlying DCM and ML depths. With a DCM much below the ML, as observed in the oligotrophic subtropical regions, the coral will record upper thermocline seawater ^{14}C records and thus $\Delta^{14}C$ reconstructed by organic nodes will underestimate surface ML values. We suggest that whilst bomb ^{14}C may reflect ML depth ^{14}C in some locations, it is not well suited to developing age models for deep-sea proteinaceous corals collected underlying sites where there is a DCM significantly below the ML, as often the case in open ocean oligotrophic regimes. Application of techniques used in this study will provide accurate and independent age models for deep-sea proteinaceous corals, opening them up as valuable palaeoceanographic archives.

Declaration of Competing Interest

The authors declare that they have no known competing financial interests or personal relationships that could have appeared to influence the work reported in this paper.

Acknowledgements

We acknowledge the crew and researchers on board the research cruise JC094 (Equatorial Atlantic in 2013) who obtained the samples for this study. We thank Oliver Andrews for his support on Earth System Model data extraction and analysis. We thank Christopher Coath, Carolyn Taylor for their help with laboratory work. We thank Abby Ren, Jesse Farmer, and an anonymous reviewer for their beneficial comments. Funding was provided by NERC grants awarded to L.F.R. (NE/S001743/1 and NE/R005117/1), China Scholarship Council to Q. L. and OCE-NSF1949984 to M.G.P.

Appendix A. Supplementary material

Research data has been also supplied via a repository: https://doi.pangaea.de/10.1594/PANGAEA.955863. Supplementary material to this article includes: Supplementary text, including

Figs. S1 and S2; research data, including Tables S1–S3. Supplementary material to this article can be found online at https://doi.org/10.1016/j.gca.2023.03.019.

References

Agustí, S., Duarte, C.M., 1999. Phytoplankton chlorophyll a distribution and water column stability in the central Atlantic Ocean. Oceanolog. Acta 22, 193–203.

Altabet, M.A., 1988. Variations in nitrogen isotopic composition between sinking and suspended particles: implications for nitrogen cycling and particle transformation in the open ocean. Deep Sea Res. Part A 35, 535–554.

Altabet, M.A., Deuser, W.G., Honjo, S., Stienen, C., 1991. Seasonal and depth-related changes in the source of sinking particles in the North Atlantic. Nature 354, 136–139.

Andrews, A.H., Stone, R.P., Lundstrom, C.C., DeVogelaere, A.P., 2009. Growth rate and age determination of bamboo corals from the northeastern Pacific Ocean using refined 210Pb dating. Mar. Ecol. Prog. Ser. 397, 173–185.

Azetsu-Scott, K., Jones, E.P., Gershey, R.M., 2005. Distribution and ventilation of water masses in the Labrador Sea inferred from CFCs and carbon tetrachloride. Mar. Chem. 94, 55–66.

Bauer, J.E., Druffel, E.R.M., Wolgast, D.M., Griffin, S., 2001. Sources and cycling of dissolved and particulate organic radiocarbon in the Northwest Atlantic Continental Margin. Global Biogeochem. Cycles 15, 615–636.

Bauer, J.E., Druffel, E.R., Wolgast, D.M., Griffin, S., 2002. Temporal and regional variability in sources and cycling of DOC and POC in the northwest Atlantic continental shelf and slope. Deep Sea Res. Part II 49, 4387–4419.

Bender, M.L., Jönsson, B., 2016. Is seasonal net community production in the South Pacific Subtropical Gyre anomalously low? Geophys. Res. Lett. 43, 9757–9763.

Bode, M., Hagen, W., Schukat, A., Teuber, L., Fonseca-Batista, D., Dehairs, F., Auel, H., 2015. Feeding strategies of tropical and subtropical calanoid copepods throughout the eastern Atlantic Ocean – Latitudinal and bathymetric aspects. Prog. Oceanogr. 138, 268–282.

Boyer, T.P., Baranova, O.K., Coleman, C., Garcia, H.E., Grodsky, A., Locarnini, R.A., Mishonov, A.V., Paver, C.R., Reagan, J.R., Seidov, D., 2018. NOAA Atlas NESDIS 87. World Ocean Database.

Broecker, W.S., Gerard, R., Ewing, M., Heezen, B.C., 1960. Natural radiocarbon in the Atlantic Ocean. J. Geophys. Res. 65, 2903–2931.

Broecker, W.S., Peng, T.H., Stuiver, M., 1978. An estimate of the upwelling rate in the equatorial Atlantic based on the distribution of bomb radiocarbon. J. Geophys. Res. 83, 6179–6186.

Brown, M.S., Munro, D.R., Feehan, C.J., Sweeney, C., Ducklow, H.W., Schofield, O.M., 2019. Enhanced oceanic CO_2 uptake along the rapidly changing West Antarctic Peninsula. Nat. Clim. Change. 9, 678–683.

Bryden, H.L., Longworth, H.R., Cunningham, S.A., 2005. Slowing of the Atlantic meridional overturning circulation at 25 degrees N. Nature 438, 655–657.

Campana, S.E., 1997. Use of radiocarbon from nuclear fallout as a dated marker in the otoliths of haddock Melanogrammus aeglefinus. Mar. Ecol. Prog. Ser. 150, 49–56.

Campana, S.E., Casselman, J.M., Jones, C.M., 2008. Bomb radiocarbon chronologies in the Arctic, with implications for the age validation of lake trout (Salvelinus namaycush) and other Arctic species. Can. J. Fish. Aquat. Sci. 65, 733–743.

Chen, T., Robinson, L.F., Burke, A., Southon, J., Spooner, P., Morris, P.J., Ng, H.C., 2015. Synchronous centennial abrupt events in the ocean and atmosphere during the last deglaciation. Science 349, 1537–1541.

Choy, E., Watanabe, K., Williams, B., Stone, R., Etnoyer, P., Druffel, E., Lorenson, T., Knaak, M., 2020. Understanding growth and age of red tree corals (Primnoa pacifica) in the North Pacific Ocean. Plos One 15, e0241692.

Claustre, H., Marty, J.-C., 1995. Specific phytoplankton biomasses and their relation to primary production in the tropical North Atlantic. Deep Sea Res. Part I 42, 1475–1493.

Claustre, H., Huot, Y., Obernosterer, I., Gentili, B., Tailliez, D., Lewis, M., 2008. Gross community production and metabolic balance in the South Pacific Gyre, using a non intrusive bio-optical method. Biogeosciences 5, 463–474.

Danabasoglu, G., 2019 NCAR CESM2-FV2 model output prepared for CMIP6 CMIP historical, Version 20201101, Earth System Grid Federation.

Deniro, M.J., Epstein, S., 1981. Influence of diet on the distribution of nitrogen isotopes in animals. Geochim. Cosmochim. Acta 45, 341–351.

Druffel, E.R.M., 1989. Decade time scale variability of ventilation in the North Atlantic: High-precision measurements of bomb radiocarbon in banded corals. J. Geophys. Res. 94, 3271–3285.

Druffel, E.R., 1996. Post-bomb radiocarbon records of surface corals from the tropical Atlantic Ocean. Radiocarbon 38, 563–572.

Druffel, E., 2002. Radiocarbon in Corals: Records of the Carbon Cycle, Surface Circulation and Climate. Oceanography 15, 122–127.

Druffel, E.M., Linick, T.W., 1978. Radiocarbon in annual coral rings of Florida. Geophys. Res. Lett. 5, 913–916.

Ellwood, M.J., Bowie, A.R., Baker, A., Gault-Ringold, M., Hassler, C., Law, C.S., Maher, W.A., Marriner, A., Nodder, S., Sander, S., Stevens, C., Townsend, A., Van Der Merwe, P., Woodward, E.M.S., Wuttig, K., Boyd, P.W., 2018. Insights Into the Biogeochemical Cycling of Iron, Nitrate, and Phosphate Across a 5,300 km South Pacific Zonal Section (153°E-150°W). Global Biogeochem. Cycles 32, 187–207.

Estrada, M., Delgado, M., Blasco, D., Latasa, M., Cabello, A.M., Benítez-Barrios, V., Fraile-Nuez, E., Mozetič, P., Vidal, M., 2016. Phytoplankton across Tropical and Subtropical Regions of the Atlantic, Indian and Pacific Oceans. PLoS One 11, e0151699.

Farmer, J.R., Robinson, L.F., Hönisch, B., 2015. Growth rate determinations from radiocarbon in bamboo corals (genus Keratoisis). Deep Sea Res. Part I 105, 26–40.

Fernandez, A., Lapen, T.J., Andreasen, R., Swart, P.K., White, C.D., Rosenheim, B.E., 2015. Ventilation time scales of the North Atlantic subtropical cell revealed by coral radiocarbon from the Cape Verde Islands. Paleoceanography 30, 938–948.

Flöter, S., Fietzke, J., Gutjahr, M., Farmer, J., Hönisch, B., Nehrke, G., Eisenhauer, A., 2019. The influence of skeletal micro-structures on potential proxy records in a bamboo coral. Geochim. Cosmochim. Acta 248, 43–60.

France, S.C., 2007. Genetic analysis of bamboo corals (Cnidaria: Octocorallia: Isididae): does lack of colony branching distinguish Lepidisis from Keratoisis? Bull. Mar. Sci. 81, 323–333.

Frenkel, M.M., LaVigne, M., Miller, H.R., Hill, T.M., McNichol, A., Gaylord, M.L., 2017. Quantifying bamboo coral growth rate nonlinearity with the radiocarbon bomb spike: A new model for paleoceanographic chronology development. Deep Sea Res. Part I. 125, 26–39.

Geyman, B.M., Ptacek, J.L., LaVigne, M., Horner, T.J., 2019. Barium in deep-sea bamboo corals: Phase associations, barium stable isotopes, & prospects for paleoceanography. Earth Planet. Sci. Lett. 525, 1–12.

Glover, H., Campbell, L., Prezelin, B., 1986. Contribution of Synechococcus spp. to size-fractioned primary productivity in three water masses in the Northwest Atlantic Ocean. Mar. Biol. 91, 193–203.

Godwin, H., 1962. Radiocarbon dating: fifth international conference. Nature 195, 943–945.

Graven, H.D., Gruber, N., Key, R., Khatiwala, S., Giraud, X., 2012. Changing controls on oceanic radiocarbon: New insights on shallow-to-deep ocean exchange and anthropogenic CO_2 uptake. J. Geophys. Res. Oceans. 117, 1–16.

Gray, J.E., 1870 Catalogue of lithophytes or stony corals in the collection of the British Museum. order of the Trustees.

Griffin, S., Druffel, E.R., 1989. Sources of carbon to deep-sea corals. Radiocarbon 31, 533–543.

Grodsky, S.A., Carton, J.A., McClain, C.R., 2008. Variability of upwelling and chlorophyll in the equatorial Atlantic. Geophys. Res. Lett. 35, 1–6.

Haskell, W.Z., Prokopenko, M.G., Stanley, R.H.R., Knapp, A.N., 2016. Estimates of vertical turbulent mixing used to determine a vertical gradient in net and gross oxygen production in the oligotrophic South Pacific Gyre. Geophys. Res. Lett. 43, 7590–7599.

Hernández-Guerra, A., Fraile-Nuez, E., López-Laatzen, F., Martínez, A., Parrilla, G., Vélez-Belchí, P., 2005. Canary Current and North Equatorial Current from an inverse box model. J. Geophys. Res. Oceans 110, 1–16.

Hill, T.M., Spero, H.J., Guilderson, T., LaVigne, M., Clague, D., Macalello, S., Jang, N., 2011. Temperature and vital effect controls on bamboo coral (Isididae) isotope geochemistry: A test of the "lines method". Geochem. Geophys. Geosyst. 12, 1–14.

Hill, T.M., Myrvold, C.R., Spero, H.J., Guilderson, T.P., 2014. Evidence for benthic–pelagic food web coupling and carbon export from California margin bamboo coral archives. Biogeosciences 11, 3845–3854.

Hirabayashi, S., Yokoyama, Y., Suzuki, A., Miyairi, Y., Aze, T., Siringan, F., Maeda, Y., 2019. Insight into Western Pacific Circulation from South China Sea Coral Skeletal Radiocarbon. Radiocarbon 61, 1923–1937.

Hobbs, W.R., Roach, C., Roy, T., Sallée, J.-B., Bindoff, N., 2021. Anthropogenic temperature and salinity changes in the Southern Ocean. J. Clim. 34, 215–228.

Kilbourne, K.H., Quinn, T.M., Guilderson, T.P., Webb, R.S., Taylor, F.W., 2007. Decadal- to interannual-scale source water variations in the Caribbean Sea recorded by Puerto Rican coral radiocarbon. Clim. Dyn. 29, 51–62.

Kimball, J.B., Dunbar, R.B., Guilderson, T.P., 2014. Oxygen and carbon isotope fractionation in calcitic deep-sea corals: Implications for paleotemperature reconstruction. Chem. Geol. 381, 223–233.

Knowles, T.D.J., Monaghan, P.S., Evershed, R.P., 2019. Radiocarbon Sample Preparation Procedures and the First Status Report from the Bristol Radiocarbon AMS (BRAMS) Facility. Radiocarbon 61, 1541–1550.

Koppelmann, R., Böttger-Schnack, R., Möbius, J., Weikert, H., 2009. Trophic relationships of zooplankton in the eastern Mediterranean based on stable isotope measurements. J. Plankton Res. 31, 669–686.

Kozak, E.R., Franco-Gordo, C., Godínez-Domínguez, E., Suárez-Morales, E., Ambriz-Arreola, I., 2020. Seasonal variability of stable isotope values and niche size in tropical calanoid copepods and zooplankton size fractions. Mar. Biol. 167.

Kromer, R.W.A.B., 2014. Temperature, salinity and other variables collected from discrete sample and profile observations using CTD, bottle and other instruments from the METEOR in the North Atlantic Ocean and South Atlantic Ocean from 1981-03-28 to 1981-04-23 (NODC Accession 0116646). Version 1.1. National Oceanographic Data Center, NOAA. Dataset.

Latasa, M., Cabello, A.M., Morán, X.A.G., Massana, R., Scharek, R., 2017. Distribution of phytoplankton groups within the deep chlorophyll maximum. Limnol. Oceanogr. 62, 665–685.

LaVigne, M., Hill, T.M., Spero, H.J., Guilderson, T.P., 2011. Bamboo coral Ba/Ca: Calibration of a new deep ocean refractory nutrient proxy. Earth Planet. Sci. Lett. 312, 506–515.

Lee, J.-M., Eltgroth, S.F., Boyle, E.A., Adkins, J.F., 2017. The transfer of bomb radiocarbon and anthropogenic lead to the deep North Atlantic Ocean observed from a deep sea coral. Earth Planet. Sci. Lett. 458, 223–232.

Macko, S.A., Wen Yuh, L., Parker, P.L., 1982. Nitrogen and carbon isotope fractionation by two species of marine amphipods: Laboratory and field studies. J. Exp. Mar. Biol. Ecol. 63, 145–149.

Marconi, D., Alexandra Weigand, M., Rafter, P.A., McIlvin, M.R., Forbes, M., Casciotti, K.L., Sigman, D.M., 2015. Nitrate isotope distributions on the US GEOTRACES North Atlantic cross-basin section: Signals of polar nitrate sources and low latitude nitrogen cycling. Mar. Chem. 177, 143–156.
Marconi, D., Weigand, M.A., Sigman, D.M., 2019. Nitrate isotopic gradients in the North Atlantic Ocean and the nitrogen isotopic composition of sinking organic matter. Deep Sea Res. Part I. 145, 109–124.
Montoya, J.P., Carpenter, E.J., Capone, D.G., 2002. Nitrogen fixation and nitrogen isotope abundances in zooplankton of the oligotrophic North Atlantic. Limnol. Oceanogr. 47, 1617–1628.
Noé, S.U., Dullo, W.C., 2006. Skeletal morphogenesis and growth mode of modern and fossil deep-water isidid gorgonians (Octocorallia) in the West Pacific (New Zealand and Sea of Okhotsk). Coral Reefs. 25, 303–320.
Olsen, A., Lange, N., Key, R.M., Tanhua, T., Álvarez, M., Becker, S., Bittig, H.C., Carter, B.R., Cotrim da Cunha, L., Feely, R.A., 2019. GLODAPv2. 2019–an update of GLODAPv2. Earth Syst. Sci. Data 11, 1437–1461.
Olsen, A., Lange, N., Key, R.M., Tanhua, T., Bittig, H.C., Kozyr, A., Àlvarez, M., Azetsu-Scott, K., Becker, S., Brown, P.J., 2020. GLODAPv2. 2020–the second update of GLODAPv2. Earth Syst. Sci. Data.
Orejas, C., Gili, J.M., Arntz, W., 2003. The role of the small planktonic communities in the diet of two Antarctic octocorals (Primnoisis antarctica and Primnoella sp.). Mar. Ecol. Prog. Ser. 250, 105–116.
Orr, J.C., Najjar, R.G., Aumont, O., Bopp, L., Bullister, J.L., Danabasoglu, G., Doney, S.C., Dunne, J.P., Dutay, J.-C., Graven, H., Griffies, S.M., John, J.G., Joos, F., Levin, I., Lindsay, K., Matear, R.J., McKinley, G.A., Mouchet, A., Oschlies, A., Romanou, A., Schlitzer, R., Tagliabue, A., Tanhua, T., Yool, A., 2017. Biogeochemical protocols and diagnostics for the CMIP6 Ocean Model Intercomparison Project (OMIP). Geosci. Model Dev. 10, 2169–2199.
Prouty, N.G., Roark, E.B., Buster, N.A., Ross, S.W., 2011. Growth rate and age distribution of deep-sea black corals in the Gulf of Mexico. Mar. Ecol. Progress Ser. 423, 101–115.
Roark, E.B., Guilderson, T.P., Flood-Page, S., Dunbar, R.B., Ingram, B.L., Fallon, S.J., McCulloch, M., 2005. Radiocarbon-based ages and growth rates of bamboo corals from the Gulf of Alaska. Geophys. Res. Lett. 32, 1–5.
Roark, E.B., Guilderson, T.P., Dunbar, R.B., Ingram, B.L., 2006. Radiocarbon-based ages and growth rates of Hawaiian deep-sea corals. Mar. Ecol. Prog. Ser. 327, 1–14.
Robinson, L.F., 2014. RRS James Cook Cruise JC094, October 13–November 30 2013, Tenerife-Trinidad. TROPICS, Tracing Oceanic Processes using Corals and Sediments. Reconstructing abrupt changes in chemistry and circulation of the equatorial Atlantic Ocean: Implications for global climate and deep-water habitats.
Romero-Romero, S., Ka'Apu-Lyons, C.A., Umhau, B.P., Benitez-Nelson, C.R., Hannides, C.C.S., Close, H.G., Drazen, J.C., Popp, B.N., 2020. Deep zooplankton rely on small particles when particle fluxes are low. Limnol. Oceanogr. Lett. 5, 410–416.
Ryan, J.P., Chavez, F.P., Bellingham, J.G., 2005. Physical-biological coupling in Monterey Bay, California: topographic influences on phytoplankton ecology. Mar. Ecol. Prog. Ser. 287, 23–32.
Saino, T., Hattori, A., 1987. Geographical variation of the water column distrubution of suspended particulate organic nitrogen and its 15N natural abundance in the Pacific and its marginal seas. Deep Sea Res. Part A Oceanogr. Res. Pap. 34, 807–827.
Schott, F.A., Mccreary, J.P., Johnson, G.C., 2004. Shallow overturning circulations of the tropical-subtropical oceans. Earth Climate: The Ocean-Atmosphere Interaction. Geophys. Monogr. 147, 261–304.
Scourse, J.D., Wanamaker, A.D., Weidman, C., Heinemeier, J., Reimer, P.J., Butler, P.G., Witbaard, R., Richardson, C.A., 2016. The Marine Radiocarbon Bomb Pulse Across the Temperate North Atlantic: A Compilation of Δ14C Time Histories from Arctica Islandic a Growth Increments. Radiocarbon 54, 165–186.
Sherwood, O.A., Edinger, E.N., 2009. Ages and growth rates of some deep-sea gorgonian and antipatharian corals of Newfoundland and Labrador. Can. J. Fish. Aquat. Sci. 66, 142–152.
Sherwood, O.A., Scott, D.B., Risk, M.J., Guilderson, T.P., 2005a. Radiocarbon evidence for annual growth rings in the deep-sea octocoral Primnoa resedaeformis. Mar. Ecol. Prog. Ser. 301, 129–134.
Sherwood, O.A., Heikoop, J.M., Scott, D.B., Risk, M.J., Guilderson, T.P., McKinney, R.A., 2005b. Stable isotopic composition of deep-sea gorgonian corals Primnoa spp.: a new archive of surface processes. Mar. Ecol. Prog. Ser. 301, 135–148.
Sherwood, O.A., Jamieson, R.E., Edinger, E.N., Wareham, V.E., 2008a. Stable C and N isotopic composition of cold-water corals from the Newfoundland and Labrador continental slope: Examination of trophic, depth and spatial effects. Deep Sea Res. Part I. 55, 1392–1402.
Sherwood, O.A., Edinger, E.N., Guilderson, T.P., Ghaleb, B., Risk, M.J., Scott, D.B., 2008b. Late Holocene radiocarbon variability in Northwest Atlantic slope waters. Earth Planet. Sci. Lett. 275, 146–153.
Sherwood, O.A., Thresher, R.E., Fallon, S.J., Davies, D.M., Trull, T.W., 2009. Multi-century time-series of 15N and 14C in bamboo corals from deep Tasmanian seamounts: evidence for stable oceanographic conditions. Mar. Ecol. Prog. Ser. 397, 209–218.
Sherwood, O.A., Lehmann, M.F., Schubert, C.J., Scott, D.B., McCarthy, M.D., 2011. Nutrient regime shift in the western North Atlantic indicated by compound-specific delta N-15 of deep-sea gorgonian corals. Proc. Natl. Acad. Sci. U.S.A. 108, 1011–1015.
Sinclair, D.J., Williams, B., Allard, G., Ghaleb, B., Fallon, S., Ross, S.W., Risk, M., 2011. Reproducibility of trace element profiles in a specimen of the deep-water bamboo coral Keratoisis sp. Geochim. Cosmochim. Acta 75, 5101–5121.
Stuiver, M., 1980. 14C distribution in the Atlantic Ocean. J. Geophys. Res. 85.
Stuiver, M., Polach, H.A., 1977. Discussion reporting of 14C data. Radiocarbon 19, 355–363.
Thresher, R.E., 2009. Environmental and compositional correlates of growth rate in deep-water bamboo corals (Gorgonacea; Isididae). Mar. Ecol. Prog. Ser. 397, 187–196.
Thresher, R.E., Fallon, S.J., 2021. Apparent Periodic and Long-Term Changes in AAIW and UCDW Properties at Fixed Depths in the Southwest Pacific, With Indications of a Regime Shift in the 1930s. Geophys. Res. Lett. 48.
Thresher, R.E., Fallon, S.J., Townsend, A.T., 2016. A "core-top" screen for trace element proxies of environmental conditions and growth rates in the calcite skeletons of bamboo corals (Isididae). Geochim. Cosmochim. Acta 193, 75–99.
Tisnérat-Laborde, N., Montagna, P., McCulloch, M., Siani, G., Silenzi, S., Frank, N., 2016. A High-Resolution Coral-Based Δ14C Record of Surface Water Processes in the Western Mediterranean Sea. Radiocarbon 55, 1617–1630.
Tracey, D., Mackay, E., Cairns, S. D., Optesko, D., Alderslade, P., Sanchez, J., Williams, G., 2014. Coral Identification Guide.
Tracey, D.M., Neil, H., Marriott, P., Andrews, A.H., Cailliet, G.M., Sanchez, J.A., 2007. Age and growth of two genera of deep-sea bamboo corals (Family Isididae) in New Zealand waters. Bull. Mar. Sci. 81, 393–408.
Ummenhofer, C.C., Murty, S.A., Sprintall, J., Lee, T., Abram, N.J., 2021. Heat and freshwater changes in the Indian Ocean region. Nat. Rev. Earth Environ., 1–17
Verrill, A.E., 1883. Report on the Anthozoa, and on some additional species dredged by the" Blake" in 1877-1879, and by the US Fish Commission steamer" Fish Hawk" in 1880-82. Museum of Comparative Zoology at Harvard College.
Wang, X.T., Prokopenko, M.G., Sigman, D.M., Adkins, J.F., Robinson, L.F., Ren, H., Oleynik, S., Williams, B., Haug, G.H., 2014. Isotopic composition of carbonate-bound organic nitrogen in deep-sea scleractinian corals: A new window into past biogeochemical change. Earth Planet. Sci. Lett. 400, 243–250.
Williams, B., 2020. Proteinaceous corals as proxy archives of paleo-environmental change. Earth Sci. Rev. 209.
Wright, E.P., 1889. Report on the Alcyonaria collected by HMS" Challenger" during the years 1873–1876. Report on the Sdentific Results of the Exploring Voyage of HMS Challenger-1873-76. ZooJogy 31, 1–43.